Volume 3 | Number 12 | December 2016

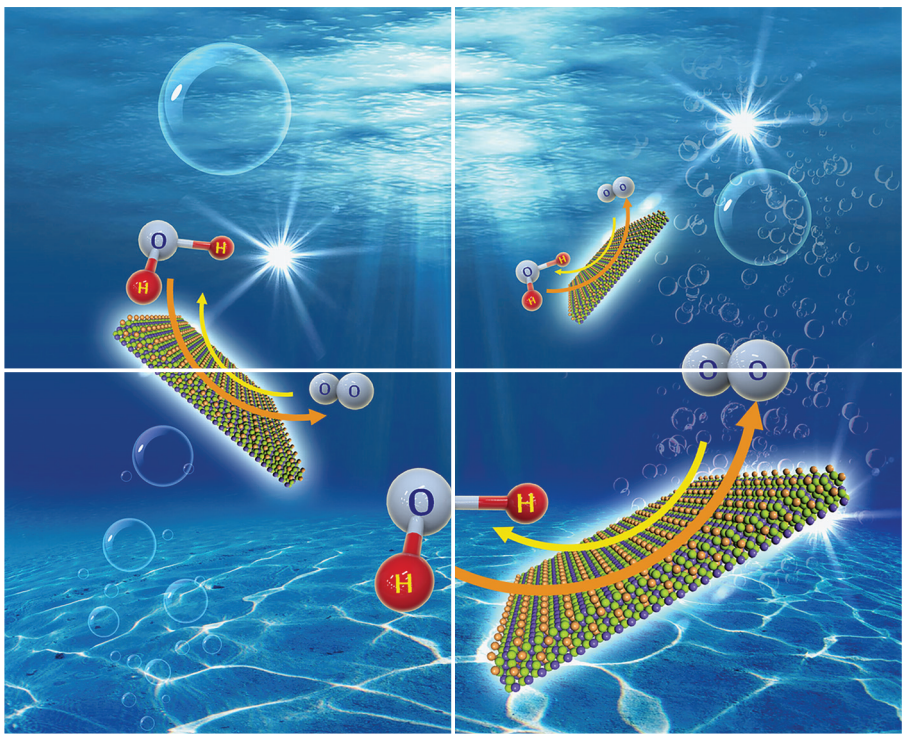

INORGANIC CHEMISTRY

FRONTIERS

Chinese Chemical Society
PEKING UNIVERSITY 1898
ROYAL SOCIETY OF CHEMISTRY

http://rsc.li/frontiers-inorganic

INORGANIC CHEMISTRY
FRONTIERS

RESEARCH ARTICLE

Cite this: *Inorg. Chem. Front.*, 2016, **3**, 1527

A microporous Cu^{2+} MOF based on a pyridyl isophthalic acid Schiff base ligand with high CO_2 uptake†‡

Andreas Kourtellaris,[a] Eleni E. Moushi,[a] Ioannis Spanopoulos,[b] Christos Tampaxis,[b,c] Georgia Charalambopoulou,[c] Theodore A. Steriotis,[c] Giannis S. Papaefstathiou,[d] Pantelis N. Trikalitis[b] and Anastasios J. Tasiopoulos*[a]

A new Cu^{2+} complex that was isolated from the initial use of 5-((pyridin-4-ylmethylene)amino)isophthalic acid ($PEIPH_2$) in 3d metal–organic framework (MOF) chemistry is reported. Complex $\{[Cu_3(PEIP)_2(5\text{-}NH_2\text{-}mBDC)(DMF)]\cdot 7DMF\}_\infty$ denoted as **Cu-PEIP**·7DMF was isolated from the reaction of $Cu(NO_3)_2\cdot 2.5H_2O$ with $PEIPH_2$ in *N*,*N*-dimethylformamide (DMF) at 100 °C and contains both the $PEIP^{2-}$ ligand and its $5\text{-}NH_2\text{-}mBDC^{2-}$ fragment. After the structure and properties of **Cu-PEIP** were known an analogous complex was prepared by a rational synthetic method that involved the reaction of $Cu(NO_3)_2\cdot 2.5H_2O$, 5-((pyridin-4-ylmethyl)amino)isophthalic acid ($PIPH_2$ – the reduced analogue of $PEIPH_2$) and $5\text{-}NH_2\text{-}mBDCH_2$ in DMF at 100 °C. **Cu-PEIP** comprises two paddle-wheel $[Cu_2(COO)_4]$ units and exhibits a 3D-framework with a unique trinodal underlying network and point symbol $(4.5^2)_4(4^2\cdot 5^4\cdot 6^4\cdot 8^3\cdot 9^2)_2(5^2\cdot 8^4)$. This network consists of pillared **kgm-a** layers containing a hexagonal shaped cavity with a relatively large diameter of ~8–9 Å surrounded by six trigonal shaped ones with a smaller diameter of ~4–5 Å and thus resembles the structure of HKUST-1. Gas sorption studies revealed that **Cu-PEIP** exhibits a 1785 $m^2\ g^{-1}$ BET area as well as high CO_2 sorption capacity (4.75 mmol g^{-1} at 273 K) and CO_2/CH_4 selectivity (8.5 at zero coverage and 273 K).

Received 25th July 2016,
Accepted 20th September 2016

DOI: 10.1039/c6qi00273k

rsc.li/frontiers-inorganic

Introduction

Metal–organic frameworks (MOFs) have attracted tremendous interest in the last decade due to their unique structural features[1] and potential applications in gas storage, separation,[2,3] magnetism,[4] catalysis,[5] sensing[6] and so on. The key factor for the discovery of MOFs with novel structural features and potentially interesting physical properties is the development of new synthetic strategies. Appropriate organic ligands are very important in this context, since even small changes in the flexibility, length, or symmetry of the ligands can result in a remarkable diversity of architectures and functions.[7,8] Although several elements of rational design have been introduced in MOF chemistry,[9] exploratory synthetic methods are still a fruitful source of novel materials with interesting properties.[10]

An apparent strategy toward new MOFs with interesting properties consists of the use of N- and O-donor polytopic organic ligands.[8a] Specifically, pyridyl-carboxylates have been confirmed as excellent ligands to assemble multidimensional coordination polymers due to the ability of the N donor atoms to bind most of the metal ions and the high bridging capability of the carboxylate groups. As a result, the carboxylate ligands can bridge several metal ions to form stable oligonuclear or polynuclear secondary building units (SBUs) which are linked through carboxylate or pyridyl N groups to afford multidimensional coordination polymers.[8a,11] One type of pyridyl polycarboxylate linkers that have attracted significant attention are the tritopic ones consisting of pyridyl and isophthalic acid moieties (for some examples see Scheme 1 in the ESI‡).[12–14] When ligands possessing the isophthalic acid moiety are employed in Cu^{2+} chemistry, they often afford structures which are similar to that of HKUST-1 with a **tbo** topology.[15] These structures either contain a layer with the **kgm-a** (augmented kagomé) or the **sql-a** (augmented square lattice) topology that are present in HKUST-1 or display an overall **tbo** topology,[12d,e,16] since the latter (**tbo**) can be regarded either as a pillared **kgm** or

[a]*Department of Chemistry, University of Cyprus, 1678 Nicosia, Cyprus. E-mail: atasio@ucy.ac.cy; Fax: +357 22895451; Tel: +357 22892765*
[b]*Department of Chemistry, University of Crete, Voutes 71003, Heraklion, Greece*
[c]*National Center for Scientific Research Demokritos, 15341 Agia Paraskevi Attikis, Greece*
[d]*Laboratory of Inorganic Chemistry, Department of Chemistry, National and Kapodistrian University of Athens, Panepistimiopolis Zografou 157 71, Greece*

†Dedicated to Professor Mercouri G. Kanatzidis on the occasion of his 60th birthday.

‡Electronic supplementary information (ESI) available: Structural figures, PXRD, IR, TGA and additional gas-sorption data. CCDC 1492970. For ESI and crystallographic data in CIF or other electronic format see DOI: 10.1039/c6qi00273k

pillared **sql** network. Thus, such ligands clearly have the potential to lead in materials resembling the structure and possibly the sorption properties of HKUST-1 and for this reason they have attracted intense interest.[12–14,16] MOFs with the **tbo** topology are highly desirable for gas sorption applications since: (a) interpenetration is not allowed and therefore high surface areas are often obtained, (b) a relatively high density of open metal sites is created, leading to high gas uptake and (c) the structure contains additional strongly interacting sites (pockets and windows) that increase the overall gas uptake.[16a]

We are interested in the use of Schiff base ligands containing the isophthalic acid group for the construction of new functional MOFs. In fact we have reported a series of MOFs based on the $CIPH_3$ ligand ($CIPH_3$ = 5-(4-carboxybenzylideneamino)isophthalic acid) with interesting single-crystal-to-single-crystal (SCSC) transformation and sorption properties.[9c,17] This ligand is more elongated than other commonly used tricarboxylic acids (such as trimesic acid) and possesses the semi-rigid C=N moiety that introduces into the isolated compounds some but not unlimited flexibility. For all these reasons $CIPH_3$ was proven capable to afford MOFs with interesting properties. As an extension of this work we employed in MOF chemistry the ligand 5-((pyridin-4-ylmethylene)amino) isophthalic acid ($PEIPH_2$) (Scheme 1 in the ESI‡) that is similar to $CIPH_3$ but contains a pyridyl group in place of the benzoic acid moiety. This ligand carries all the advantages of the other pyridyl-isophthalic acid linkers mentioned above and displays unpredictable behavior when it is involved in reactions with metal ion sources. This arises from the fact that both $PEIPH_2$ and its constituent moieties are present in the solution containing the ligand and thus it is possible for them to appear in the resulting compounds giving rise to a variety of new products. Surprisingly the coordination chemistry of $PEIPH_2$ is actually unexplored with the only known compounds with this ligand being some organotin MOFs.[14]

We herein report a new Cu^{2+} MOF $\{[Cu_3(PEIP)_2(5\text{-}NH_2\text{-}mBDC)(DMF)]\cdot 7DMF\}_\infty$ denoted as **Cu-PEIP**·7DMF which represents the initial 3d metal complex with the ligand $PEIPH_2$. Although this compound was prepared by a serendipitous self-assembly synthetic procedure, after its structure was known the synthesis of an analogous complex was targeted with high priority and achieved following a rational synthetic method. **Cu-PEIP** exhibits a 3D-framework with a unique trinodal underlying network and point symbol $(4\cdot5^2)_4(4^2\cdot5^4\cdot6^4\cdot8^3\cdot9^2)_2(5^2\cdot8^4)$. This network consists of pillared **kgm-a** layers and thus resembles the structure of HKUST-1. **Cu-PEIP** shows a significant BET area (1785 $m^2\ g^{-1}$) as well as high CO_2 sorption capacity (4.75 mmol g^{-1} at 273 K) and CO_2/CH_4 selectivity (8.5 at zero coverage and 273 K).

Experimental

Materials

Reagent grade chemicals were obtained from Aldrich and used without further purification. Water was distilled in-house. $PEIPH_2$ and $PIPH_2$ were synthesized according to the reported literature.[13d,14]

Synthesis of Cu-PEIP

Method A: $PEIPH_2$ (0.08 g, 0.296 mmol) was dissolved (after sonication for 3 minutes) in 5 mL *N*,*N*-dimethylformamide (DMF) in a 20 mL glass vial and solid $Cu(NO_3)_2\cdot 2.5H_2O$ (0.08 g, 0.344 mmol) was added to this solution. The mixture was sonicated for 3 min, sealed and then, heated without stirring at 100 °C for 24 h. During this period, green polyhedral-like crystals of **Cu-PEIP** were formed. They were isolated by filtration, washed several times with DMF and diethylether, and dried under vacuum. The yield was 70%. Elemental analysis: Anal. Calc. for $C_{60}H_{77}O_{20}N_{13}Cu_3$ (**Cu-PEIP**·7DMF) C 48.34, H 5.21, N 12.21, Found: C 48.23, H 5.11, N 12.09.

Method B: Method A was repeated, using 5-NH_2-m$BDCH_2$ (0.08 g, 0.442 mmol) and 4-pyridinecarboxaldehyde (43 μL, 0.456 mmol) instead of $PEIPH_2$. The yield was ~65%.

Synthesis of Cu-PIP

$PIPH_2$ (0.08 g, 0.294 mmol) and 5-NH_2-m$BDCH_2$ (0.05 g, 0.276 mmol) were dissolved (after sonication for 3 minutes) in DMF (5 mL) in a 20 mL glass vial and solid $Cu(NO_3)_2\cdot 2.5H_2O$ (0.08 g, 0.344 mmol) was added to this solution. The mixture was sonicated for 3 min, sealed and then, heated without stirring at 100 °C for 24 h. During this period, green crystalline solid of **Cu-PIP** was formed. The microcrystalline solid was isolated by filtration, washed several times with DMF and diethylether, and dried under vacuum. The yield was 46%. Anal. Calc. for $C_{60}H_{81}O_{20}N_{13}Cu_3$ (**Cu-PIP**·7DMF) C 48.20, H 5.46, N 12.18, Found: C 47.94, H 5.36, N 12.03.

Physical measurements

Elemental analysis (C, H, N) was performed by the in-house facilities of the University of Cyprus, Chemistry Department. IR spectra were recorded on KBr pellets in the 4000–400 cm^{-1} range using a Shimadzu Prestige -21 spectrometer. PXRD patterns were recorded on a Shimazdu 6000 Series X-ray diffractometer (Cu Kα radiation, λ = 1.5418 Å). Thermal stability studies were performed with a Shimadzu TGA 50 thermogravimetric analyzer.

Gas sorption measurements

Low-pressure argon, hydrogen, carbon dioxide and methane adsorption measurements were carried out on an Autosorb 1-MP instrument from Quantachrome equipped with multiple pressure transducers for highly accurate analyses and an oil-free vacuum system. High pressure excess adsorption measurements were conducted manometrically on a PCTPro-2000 instrument (Setaram) with the aid of a regular valve sealed stainless-steel measuring cell. The NIST database was implemented for estimating the compressibility of gases (H_2, CH_4, CO_2) and helium was used for dead volume calibrations at 273–303 K. In order to avoid potential helium sorption errors, the dead volume at 77 K was calculated through a reference curve obtained by using different volumes

of non-adsorbing materials (Pyrex glass). Ultra-high purity grade Ar (99.999%), He (99.999%), H_2 (99.999%), CO_2 (99.999%) and CH_4 (99.9995%) were used for all adsorption measurements. Prior to analysis, as-made **Cu-PEIP** was soaked in CH_2Cl_2 at room temperature for three (3) days during which the supernatant solution was replaced six (6) times. The dichloromethane suspended samples were transferred inside the chamber of a supercritical CO_2 dryer (Bal-Tec CPD 030) and CH_2Cl_2 was exchanged with liquid CO_2 over a period of 5 hours at 8 °C. During this period, liquid CO_2 was vented under positive pressure every 5 minutes. The rate of CO_2 venting was always kept below the rate of filling so as to maintain full drying conditions inside the chamber. Following venting, the temperature was raised to 40 °C (above the critical temperature of CO_2), kept there for 1 hour and then slowly vented over the period of 1 hour. The dried sample was transferred immediately inside a pre-weighted, argon filled 9 mm cell and closed using CellSeal™ provided by Quantachrome to prevent the intrusion of oxygen and atmospheric moisture during transfers and weighing. The cell was then transferred to the outgassing station where the sample was evacuated under dynamic vacuum at room temperature until the outgas rate was less than 2 mTorr min^{-1}. After evacuation, the sample and cell were re-weighed to obtain the precise mass of the evacuated sample. Finally, the tube was transferred to the analysis port of the gas adsorption instrument. Likewise, for high pressure measurements, the dried sample was transferred sealed to an argon filled glove box (Labstar, MBraun, H_2O and O_2 <0.5 ppm), and a quantity of approx. 180 mg was inserted into a pre-weighted stainless-steel container. The sample mass was calculated and the container was sealed with a high pressure valve. The whole cell was removed from the glove box and was attached to the high pressure manometric apparatus. All-metal face seals were used. After suitable evacuation of the apparatus the sample was further outgassed overnight at room temperature under high vacuum ($p < 10^{-6}$ mbar). The outgassing procedure was repeated after each high pressure measurement.

Single crystal X-ray crystallography

Single crystal X-ray diffraction data were collected on an Oxford-Diffraction Supernova diffractometer, equipped with a CCD area detector utilizing Cu Kα (λ = 1.5418 Å) radiation. A suitable crystal was mounted on a Hampton cryoloop with Paratone-N oil and transferred to a goniostat where it was cooled for data collection. Empirical absorption corrections (multiscan based on symmetry-related measurements) were applied using CrysAlis RED software.[18] The structure was solved by direct methods using SIR2004[19] and refined on F^2 using full-matrix least-squares with SHELXL97.[20] Software packages used were as follows: CrysAlis CCD for data collection,[18] CrysAlis RED for cell refinement and data reduction,[18] WINGX for geometric calculations,[21] and DIAMOND[22] and X-Seed[23] for molecular graphics. The non-H atoms were treated anisotropically, whereas the aromatic H atoms were placed in calculated, ideal positions and refined as riding on their respective carbon atoms. Electron density contributions from disordered guest molecules were handled using the SQUEEZE procedure from the PLATON software suit.[24] Selected crystal data for **Cu-PEIP** are summarized in Table 1. CCDC 1492970 contains the supplementary crystallographic data for this paper.

Table 1 Selected crystal data for **Cu-PEIP**

Complex	Cu-PEIP
Empirical formula	$C_{39}H_{25}Cu_3N_6O_{13}$
Formula weight	976.30
Temperature (K)	100(2)
Radiation	Cu Kα (λ = 1.54180 Å)
Crystal system	Monoclinic
Space group	*I*2/*m*
a (Å)	13.657(5)
b (Å)	18.686(5)
c (Å)	31.503(5)
β (°)	101.532(5)
V (Å^3)	7877(4)
Z	4
D_c (g cm^{-3})	0.823
μ (mm^{-1})	1.266
Refls coll.	27 001
Unique refls	7255
R_{int}	0.0367
R_1 [a] [$I > 2\sigma(I)$]	0.0749
wR_2 [b] (all data)	0.2441
GOF	1.157
$\Delta\rho_{min/max}$ (e Å^3)	1.279/−0.658

[a] $R_1 = \sum||F_o| - |F_c||/\sum|F_o|$. [b] $wR_2 = \{\sum[w(|F_o|^2 - |F_c|^2)^2]/\sum[w(|F_o|^4)]\}^{1/2}$.

Results and discussion

Over the last few years, we have been systematically investigating the use of semi-rigid polytopic ligands, such as $CIPH_3$ as a method for the synthesis of new MOFs.[9c,17] An extension of these investigations included the use of $PEIPH_2$, which is similar to $CIPH_3$ but contains a pyridyl group in the place of the benzoic acid moiety, in MOF chemistry. Compound **Cu-PEIP** was initially prepared from the reaction of $Cu(NO_3)_2{\cdot}2.5H_2O$ and $PEIPH_2$ in DMF at 100 °C in 70% yield. A similar reaction was performed that contained instead of the pre-formed Schiff base ligand $PEIPH_2$ its constituent moieties, *i.e.* 5-NH_2-$mBDCH_2$ and 4-pyridinecarboxaldehyde aiming at the *in situ* formation of the ligand and the isolation of the final product through a one-pot reaction (by omitting the ligand preparation step). This was realized from the reaction of $Cu(NO_3)_2{\cdot}2.5H_2O$, 5-NH_2-$mBDCH_2$ and 4-pyridinecarboxaldehyde in DMF at 100 °C in 65% yield. Interestingly, **Cu-PEIP** was isolated as excellent quality green polyhedral-like crystals in very high yields with both synthetic methods. When the structure of the compound **Cu-PEIP** was known the synthesis of an analogous complex was targeted and achieved by following a rational synthetic procedure. This procedure involved the use in the reaction mixture of the reduced analogue of $PEIPH_2$, *i.e.* ligand $PIPH_2$ that remains intact in solution, and 5-NH_2-$mBDCH_2$. Thus, compound **Cu-PIP** was prepared from the

reaction of $Cu(NO_3)_2{\cdot}2.5H_2O$, $PIPH_2$ and 5-NH_2-$mBDCH_2$ in DMF at 100 °C in 46% yield. The identity and purity of the bulk products of **Cu-PEIP** and **Cu-PIP** and their structural relation were confirmed by PXRD, elemental analysis and infrared spectroscopy (Fig. S1–S4 in the ESI‡).

Compound **Cu-PEIP** crystallizes in the monoclinic space group *I*2/*m*. There are two crystallographically unique Cu^{2+} ions in the structure (Cu1 and Cu2), both adopting a square pyramidal coordination geometry (Fig. 1): Cu1 is coordinated with four carboxylic oxygen atoms 2 × (O1–O2) of four different $PEIP^{2-}$ ligands and one terminal DMF (O7) solvent molecule, whereas Cu2 is connected with two carboxylate oxygen atoms (O3–O4) from two different $PEIP^{2-}$ anions, two carboxylate oxygen atoms (O5–O6) from two different 5-NH_2-$mBDC^{2-}$ ligands and one nitrogen atom from a third $PEIP^{2-}$ ligand (N1). This connectivity gives rise to a 3-D framework, which comprises two paddle-wheel $[Cu_2(COO)_4]$ SBUs and exhibits large channels running mainly along the *a*-axis (Fig. 2a). The first type of dinuclear SBU, $[Cu_2]_A$, is formed by two symmetry-equivalent Cu1 metal ions, which are bridged by four *syn*,*syn*-μ_2-COO^- groups originating from four $PEIP^{2-}$ ligands, whereas the second paddle-wheel type SBU, $[Cu_2]_B$, consists of two symmetry-equivalent Cu2 ions, which are bridged by four *syn*,*syn*-μ_2-COO^- groups originating from two $PEIP^{2-}$ and two 5-NH_2-$mBDC^{2-}$ ligands. The axial positions in $[Cu_2]_A$ are occupied by two oxygen atoms from two DMF molecules, while those in $[Cu_2]_B$ by two pyridyl nitrogen atoms from two $PEIP^{2-}$ ligands. The 5-NH_2-$mBDC^{2-}$ ligands bridge two $[Cu_2]_B$ SBUs with a $[Cu_2]_B\cdots[Cu_2]_B$ separation of ~9.3 Å while the isophthalate moiety of the $PEIP^{2-}$ ligands bridges a $[Cu_2]_A$ to a $[Cu_2]_B$ SBU with the $[Cu_2]_A\cdots[Cu_2]_B$ separation being ~9.2 Å. In this arrangement, the paddle-wheels and the isophthalate moieties of both ligands create an undulated (3·6·3·6) semi-regular plane net (**kgm-a** lattice) parallel to the *bc* plane (Fig. 2b). This layer contains two types of cavities; a hexagonal shaped with a relatively large diameter of ~8–9 Å surrounded by six trigonal shaped ones with a smaller diameter of ~4–5 Å as found by PLATON[24] (taking into account the van der Waals radii of the atoms). The trigonal shaped cavities are composed of one $[Cu_2]_A$ and two $[Cu_2]_B$ SBUs and are filled with the terminal DMF molecules bound to $[Cu_2]_A$ SBUs. The hexagonal shaped cavities are composed of two $[Cu_2]_A$ separating two pairs of two $[Cu_2]_B$ SBUs. The sides of the hexagonal cavities comprise the isophthalate moieties of two approximately parallel 5-NH_2-$mBDC^{2-}$ ligands separating two adjacent isophthalate moieties of two pairs of $PEIP^{2-}$ ligands.

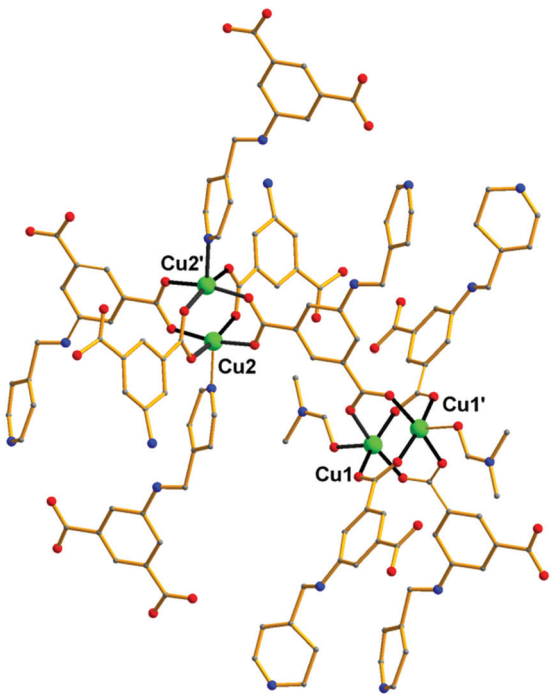

Fig. 1 Representation of the connectivity of the $[Cu^{2+}]_2$ paddle wheel SBUs through the $PEIP^{2-}$ ligand in **Cu-PEIP**. Colour code: Cu green, O red, N blue, C gray. H atoms are omitted for clarity.

The **kgm-a** layers are pillared through the pyridyl groups of the $PEIP^{2-}$ ligands giving rise to hexagonal channels running parallel to the *a* axis (Fig. 2c and d). Since there are only four $PEIP^{2-}$ ligands composing the hexagonal cavities, only four $[Cu_2]_B$ SBUs act as connection points in the pillaring. The 5-NH_2-$mBDC^{2-}$ ligands point their amino group toward the hexagonal cavities, thus compartmentalizing the cavities and the hexagonal channels as shown in Fig. 2c and d. Since part of the isophthalate ligands and part of the $[Cu_2]$ SBUs participate in the pillaring there is enough space left uncovered giving rise to pores through the other two directions of the material. The pores accommodate DMF molecules.

The solvent-accessible volume calculated by PLATON[24] is 5241 $Å^3$ and corresponds to 66.5% of the unit-cell volume (7877.0 $Å^3$). A representation of the voids using the structure visualization program MERCURY[25] reveals a continuous and complex 3D pore network, where the large compartmentalized hexagonal cavities communicate through relatively wide channels with a diameter ≥4 Å (Fig. 3).

From the topological point of view the $[Cu_2]_A$ paddle-wheel SBUs possessing two DMF molecules on the Cu1 apical sites serve as 4-coordinated nodes, while the $[Cu_2]_B$ SBUs possessing two pyridyl N atoms on the apical positions of the Cu2 ions act as 6-c nodes. The $PEIP^{2-}$ ligands bridge a $[Cu_2]_A$ to a $[Cu_2]_B$ through the isophthalate moiety and a $[Cu_2]_B$ through the pyridyl N atom, thus serving as a 3-c node. The 5-NH_2-$mBDC^{2-}$ ligand simply bridges two $[Cu_2]_B$ SBUs and therefore is topologically silent (serves as a bridge). In this arrangement a 3,4,6-coordinated trinodal network with the stoichiometry $(3\text{-c})_4(4\text{-c})(6\text{-c})_2$ and point symbol $(4{\cdot}5^2)_4(4^2{\cdot}5^4{\cdot}6^4{\cdot}8^3{\cdot}9^2)_2(5^2{\cdot}8^4)$ forms which is, so far, unique (Fig. S5–S8 in the ESI‡). The network adopted by **Cu-PEIP** resembles the **tbo** net adopted by HKUST-1 and the **eea** net.[12d,e,15,16] All three nets can be considered as pillared **kgm-a** layers. The augmented Kagomé lattice (**kgm-a**) is based on $[Cu_2(COO)_4]$ SBUs and isophthalate moieties which alternate to create big hexagonal cavities comprising six paddle-wheels and six isophthalate moieties. In **tbo** the **kgm-a** layers are separated (pillared) by the third carboxylate of the trimesic acid while in the **eea** net the layers are

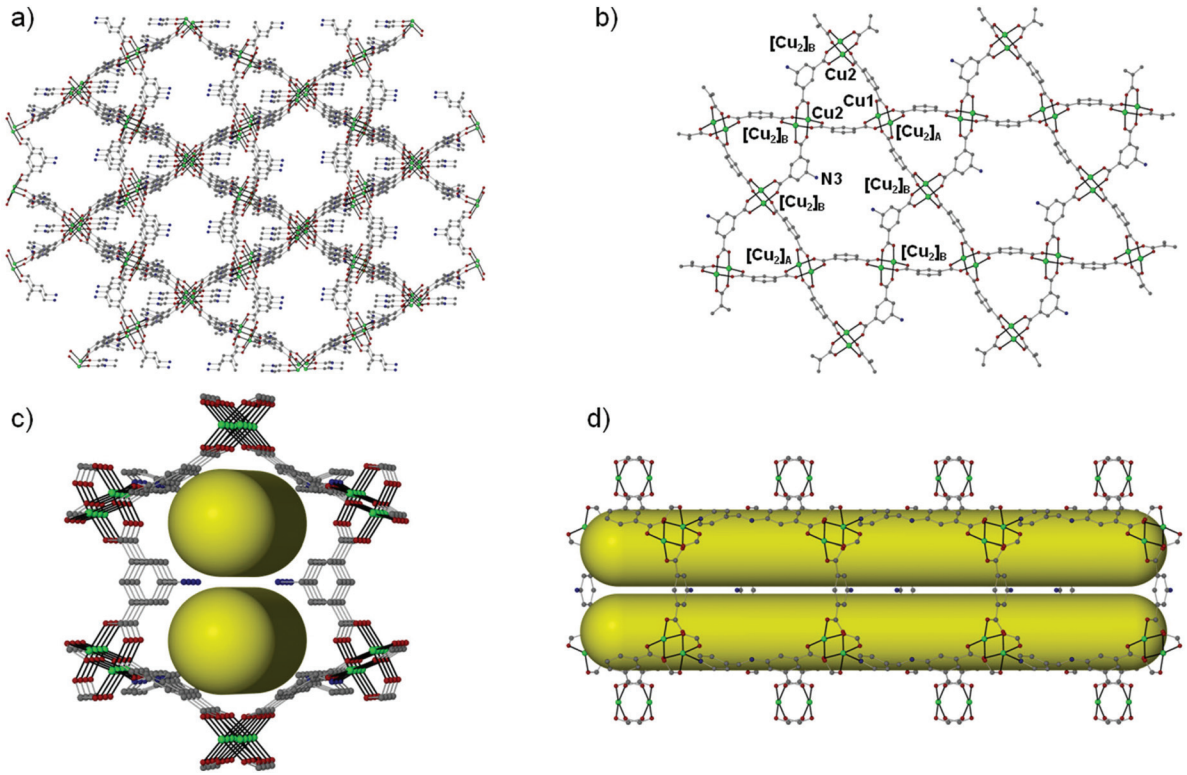

Fig. 2 Representations of (a) the 3D framework along the *a* axis, (b) the (3·6·3·6) semi-regular net (augmented Kagomé lattice: **kgm-a**), (c) the compartmentalized hexagonal channels along the *a* axis and (d) the compartmentalized channel projected along the *a* axis for complex **Cu-PEIP**. Colour code: Cu green, O red, N blue, C gray. H atoms are omitted for clarity.

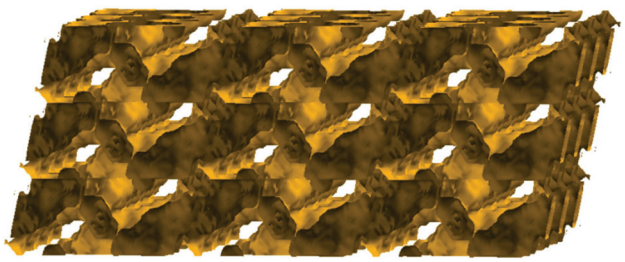

Fig. 3 Representation of the pore network (shown in yellow) of **Cu-PEIP** (only pores and channels with diameter ≥4 Å are shown) along the *b* axis.

separated by the pending pyridyl groups of the pyridyl-isophthalate ligands. In both **tbo** and **eea** nets, all six bridging ligands around each hexagonal cavity serve as pillars to both sides of the layer while in **Cu-PEIP** only four $PEIP^{2-}$ ligands serve as pillars since two out of the six bridges around the hexagonal cavities are 5-NH_2-$mBDC^{2-}$ ligands which cannot connect neighboring **kgm-a** layers.

The thermal stability of **Cu-PEIP** and **Cu-PIP** was investigated by means of the thermogravimetric analysis (TGA) technique (Fig. S9 and S10 in the ESI‡). The TGA curves for the two complexes are essentially identical and thus only that of **Cu-PEIP** shall be discussed in detail. The TGA curve of **Cu-PEIP** indicates that this compound is decomposed through a multi-step process which is completed at a fairly low temperature (~400 °C). The first two steps that are related to the removal of the lattice and bound DMF solvent molecules appear in the temperature range 30 °C to 260 °C and correspond to ~40% of the material's total mass. This value is in agreement with the corresponding calculated value for **Cu-PEIP**·7DMF (~39.2%). The next steps are associated with the decomposition of the two bridging ligands $PEIP^{2-}$ and 5-NH_2-$mBDC^{2-}$ and are completed at ~400 °C.

The relatively large solvent accessible volume present in **Cu-PEIP** prompted us to investigate its gas sorption properties. Several activation methods were employed, however the most efficient one involved the use of dichloromethane to remove the guest solvent molecules followed by treatment with supercritical CO_2. Argon sorption measurements at 87 K revealed a type-I isotherm (Fig. 4), typical for a microporous solid, from which the apparent BET area was found to be 1785 $m^2\ g^{-1}$ (Langmuir, 1814 $m^2\ g^{-1}$), close to the geometric surface area (2059 $m^2\ g^{-1}$) calculated from the single crystal structure using Poreblazer.[26] The total pore volume is 0.64 $cm^3\ g^{-1}$ at relative pressure, p/p_o, 0.99, which is slightly lower compared to the value of 0.75 $cm^3\ g^{-1}$ calculated[26] from the crystal structure. Given that the PXRD pattern of the activated sample suggests an intact framework, the difference in the pore volume could be explained by trapped organic molecules inside the pores of **Cu-PEIP**. The pore size distribution, calculated using Non-

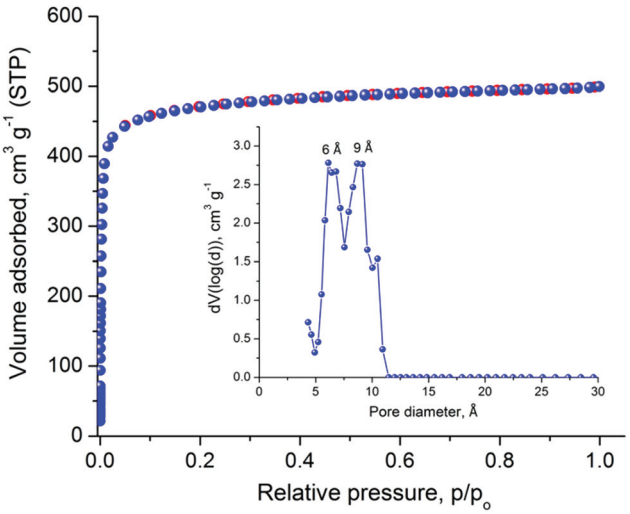

Fig. 4 Argon sorption isotherm of **Cu-PEIP** recorded at 87 K and pore size distribution curve calculated by NLDFT (inset).

Local Density Functional Theory (NLDFT) after a successful fitting of the Ar adsorption isotherm data using a suitable NLDFT kernel (Fig. S11 in the ESI‡), shows two major peaks centered at 6 Å and 9 Å (inset in Fig. 4), in agreement with the crystallographic analysis.

The high porosity of **Cu-PEIP** in combination with the presence of unsaturated Cu(II) sites and $-NH_2$ groups, prompted us to further investigate the gas sorption properties by recording low and high pressure isotherms of CO_2, CH_4 and H_2 at different temperatures from which the total uptake, isosteric heat of adsorption (Q_{st}) and CO_2/CH_4, selectivity were calculated. We note that amine functionalized MOFs are highly desirable, especially for CO_2 capture, because high uptake and selectivity are expected due to favorable acid–base interactions.[27]

The CO_2 uptake at 1 bar is 4.75 mmol g^{-1} (20.9 wt%) and 2.80 mmol g^{-1} (12.3 wt%) at 273 K and 298 K, respectively (Fig. 5). These values are within the same range of representative and high performance NH_2-functionalized MOFs including NH_2-MIL-101(Cr) (3.2 and 1.9 mmol g^{-1} at 273 K and 298 K),[28] $Zn(Atz)_2$ (4.35 mmol g^{-1} at 1.2 bar and 273 K),[29] NH_2-MIL-125(Ti) (5.9 mmol g^{-1} at 273 K)[30] and NH_2-UiO-66 (between 2.89 and 3.04 mmol g^{-1} at 298 K).[31] The isosteric heat of adsorption, Q_{st}, was calculated to be 34.2 kJ mol^{-1} at zero coverage (Fig. 6 and S12). Such a moderate value, which is lower compared to some NH_2-functionalized MOFs, such as NH_2-MIL-101(Cr) (52 kJ mol^{-1})[28] and $Zn(Atz)_2$ (40.8 kJ mol^{-1}),[29] is highly desirable because of the anticipated lower regeneration energy demand.[27] At elevated pressures, very high gravimetric and volumetric CO_2 uptake is observed, reaching 317 cm^3 g^{-1} (14.2 mmol g^{-1}) and 242 cm^3 cm^{-3}, respectively, at 298 K and 25 bar, while the corresponding saturation uptake at 50 bar is 347 cm^3 g^{-1} (15.5 mmol g^{-1}) and 264 cm^3 g^{-1} (Fig. 5b). For comparison, the observed volumetric uptake at 25 bar and 298 K is slightly lower than MOF-177 (273 cm^3 cm^{-3}),[32] HKUST-1 (276 cm^3 cm^{-3})[33] and Mg-MOF-74 (285 cm^3 cm^{-3})[34] but higher than MOF-5 (225 cm^3 cm^{-3}),[32] gea-MOF-1 (224 cm^3 cm^{-3}),[35] MOF-210 (127 cm^3 cm^{-3})[32] and MOF-200 (112 cm^3 cm^{-3}).[32]

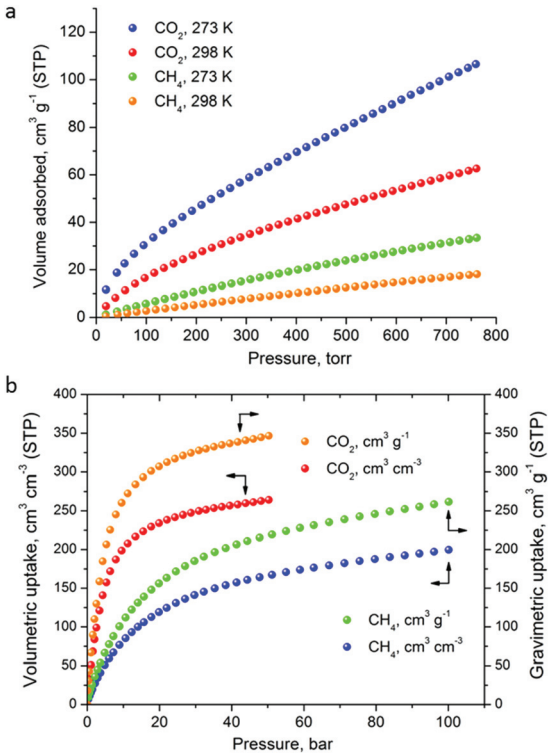

Fig. 5 (a) Low pressure CO_2 and CH_4 sorption isotherms of **Cu-PEIP** at the indicated temperatures, up to 1 bar. (b) The corresponding high pressure isotherms recorded at 298 K.

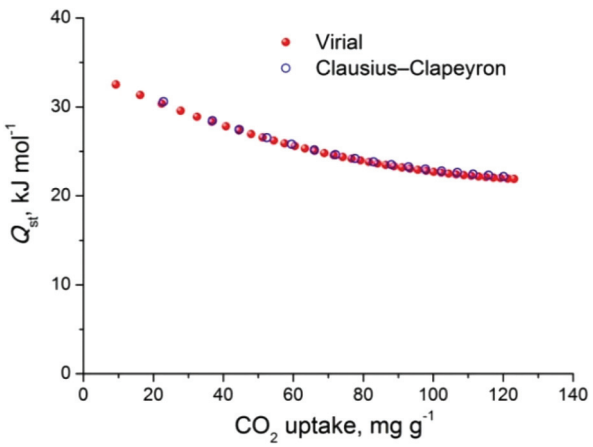

Fig. 6 CO_2 isosteric heat of adsorption (Q_{st}) in **Cu-PEIP** as a function of surface coverage, calculated from a virial-type analysis. The corresponding Clausius–Clapeyron calculation is also shown, for comparison.

The CH_4 adsorption isotherms up to 1 bar, shown in Fig. 5a revealed an uptake of 33.4 cm^3 g^{-1} (1.49 mmol g^{-1}) and 18.1 cm^3 g^{-1} (0.81 mmol g^{-1}) at 273 K and 298 K, respectively. From these isotherms, the calculated isosteric heat of adsorption, Q_{st}, at zero coverage using a virial-type equation, was

estimated to be 21.2 kJ mol^{-1} and remained nearly constant as a function of the surface coverage (Fig. S13 and S14‡). Interestingly, this value is higher compared to HKUST-1 (17 kJ mol^{-1}) and among the highest reported for MOFs (Table S1‡).[36,37] For example, Ni-MOF-74 with a very high density of open metal sites showed a Q_{st} value of 21.4 kJ mol^{-1}.[36] Very recently, a novel MOF without open metal sites, denoted as MAF-38, showed a Q_{st} value of 21.6 kJ mol^{-1} at zero coverage.[38] Despite the high Q_{st} value for **Cu-PEIP**, a relatively high CO_2/CH_4 selectivity at low pressures, calculated using the IAST model, is observed reaching 8.5 at 273 K and 8.9 at 298 K.

High-pressure CH_4 measurements revealed that the total gravimetric (cm^3 g^{-1}) and volumetric (cm^3 cm^{-3}) uptake at 298 K, is 197 and 150 at 35 bar, 233 and 176 at 65 bar and 246 and 187 at 80 bar, respectively. The resulting gravimetric CH_4 working storage capacities in the pressure ranges 5–35 bar (US DOE standard),[39] 5–65 bar and 5–80 bar are estimated to be 131 cm^3 g^{-1}, 167 cm^3 g^{-1} and 180 cm^3 g^{-1}, respectively. The corresponding volumetric working capacities are 99 cm^3 cm^{-3}, 125 cm^3 cm^{-3} and 136 cm^3 cm^{-3}. These values are lower compared to the best performing MOFs (Tables S1 and S2 in the ESI‡) due to the combination of high Q_{st} and a moderate surface area in **Cu-PEIP**. Compared to Ni-MOF-74, a MOF with a high Q_{st} for CH_4 and a slightly lower BET area (1350 m^2 g^{-1}), **Cu-PEIP** performs better in terms of the gravimetric working capacity at 5–65 bar (0.110 *vs.* 0.077 g g^{-1}) and 5–80 bar (0.129 *vs.* 0.091 g g^{-1}) (Tables S1 and S2 in the ESI‡).

Low pressure, H_2 sorption isotherms recorded up to 1 bar at 77 K and 87 K revealed an uptake of 206 cm^3 g^{-1} (2.06 wt%) and 143 cm^3 g^{-1} (1.43 wt%), respectively, which is higher than the benchmark MOF-177 (142 and 82 cm^3 g^{-1}) (Fig. S15‡).[40] The calculated Q_{st} at zero coverage is 8.74 kJ mol^{-1} (Fig. S16 and S17‡), which is significantly higher than some well-known and high performance MOFs[41] including MOF-5 and MOF-177 (4.4 kJ mol^{-1}).[40] High pressure H_2 measurements, revealed an uptake of 614 cm^3 g^{-1} (5.5 wt%) which is lower than the ultra-high surface area MOFs such as MOF-210 and NU-100 (Fig. S18‡). However, at 20 bar, due to a high Q_{st}, the uptake is 4.1 wt%, comparable to the best performing MOFs.

Conclusions

Summarizing, a new Cu^{2+} MOF is reported that was isolated from the initial use of ligand $PEIPH_2$ in 3d MOF chemistry. Interestingly, **Cu-PEIP** displays novel structural features although pyridyl isophthalic acid tritopic ligands have been extensively employed in Cu MOF chemistry due to their ability to afford MOFs that display structural similarity with HKUST-1. The unique structural features of **Cu-PEIP** arose from the presence in its structure of both $PEIPH_2$ and 5-NH_2-$mBDCH_2$ due to the capability of the tritopic Schiff base ligand to partially decompose in solution and appear in the reaction mixture together with its constituent moieties. After the structure of **Cu-PEIP** was known the synthesis of an analogous compound was targeted and achieved by employing a rational synthetic procedure. The crystal structure of **Cu-PEIP** exhibits a 3D-framework that contains large pores (~9 Å) and solvent accessible volume (~66.5%). In addition, it displays a unique trinodal underlying network consisting of pillared **kgm-a** layers and thus resembles the structure of HKUST-1. Gas sorption studies revealed that **Cu-PEIP** displays a significant BET area of 1785 m^2 g^{-1} and high CO_2 uptake, reaching 4.75 mmol g^{-1} at 273 K and 1 bar (2.80 mmol g^{-1} at 298 K) with good CO_2/CH_4 selectivity (8.5/8.9 at 273 K/298 K). Furthermore, high pressure gas sorption studies revealed that the volumetric CO_2 uptake at 25 bar (242 cm^3 cm^{-3} at 298 K) is higher compared to representative high surface area MOFs, including MOF-5, MOF-200 and MOF-210. This study emphasizes the usefulness of the elements of serendipity introduced from the employment of polytopic Schiff base ligands in MOF chemistry for the synthesis of microporous MOFs with unique structural features and interesting sorption properties. Further investigations are in progress focusing on the isolation of **Cu-PEIP** analogues containing various functionalized derivatives of isophthalic acid and/or more elongated tritopic pyridyl isophthalic acid ligands.

Acknowledgements

This work was supported by the Cyprus Research Promotion Foundation Grant ΔΙΔΑΚΤΩΡ/0609/43 which is co-funded by the Republic of Cyprus and the European Regional Development Fund. EM and AJT thank the University of Cyprus for an internal postdoctoral fellowship to EM.

Notes and references

1 (*a*) M. Eddaoudi, D. B. Moler, H. Li, B. Chen, T. M. Reineke, M. O'Keeffe and O. M. Yaghi, *Acc. Chem. Res.*, 2001, **34**, 319–330; (*b*) D. Bradshaw, J. B. Claridge, E. J. Cussen, T. J. Prior and M. J. Rosseinsky, *Acc. Chem. Res.*, 2005, **38**, 273–282; (*c*) G. Ferey, *Chem. Soc. Rev.*, 2008, **37**, 191–214.

2 (*a*) N. L. Rosi, J. Eckert, M. Eddaoudi, D. T. Vodak, J. Kim, M. O'Keeffe and O. M. Yaghi, *Science*, 2003, **300**, 1127–1129; (*b*) S. Zheng, T. Wu, J. Zhang, M. Chow, R. A. Nieto, P. Feng and X. H. Bu, *Angew. Chem., Int. Ed.*, 2010, **49**, 5362–5366; (*c*) B. F. Abrahams, M. J. Grannas, T. A. Hudson and R. Robson, *Angew. Chem., Int. Ed.*, 2010, **49**, 1087–1089.

3 (*a*) H. Hayashi, A. P. Cote, H. Furukawa, M. O'Keeffe and O. M. Yaghi, *Nat. Mater.*, 2007, **6**, 501–506; (*b*) R. E. Morris and P. S. Wheatley, *Angew. Chem., Int. Ed.*, 2008, **47**, 4966–4981; (*c*) S. Noro, S. Kitagawa, M. Kondo and K. Seki, *Angew. Chem., Int. Ed.*, 2000, **39**, 2081–2084.

4 (*a*) E. E. Moushi, T. C. Stamatatos, W. Wernsdorfer, V. Nastopoulos, G. Christou and A. J. Tasiopoulos, *Angew. Chem., Int. Ed.*, 2006, **45**, 7722–7725; (*b*) P. Dechambenoit and J. R. Long, *Chem. Soc. Rev.*, 2011, **40**, 3249–3265.

5 (*a*) L. Ma, J. M. Falkowski, C. Abney and W. Lin, *Nat. Chem.*, 2010, **2**, 838–846; (*b*) J.-S. Qin, D.-Y. Du, W. Guan, X.-J. Bo, Y.-F. Li, L.-P. Guo, Z.-M. Su, Y.-Y. Wang, Y.-Q. Lan and H.-C. Zhou, *J. Am. Chem. Soc.*, 2015, **137**, 7169–7177.

6 (*a*) Z. Hu, B. J. Deibert and J. Li, *Chem. Soc. Rev.*, 2014, **43**, 5815–5840; (*b*) A. Douvali, A. C. Tsipis, S. V. Eliseeva, S. Petoud, G. S. Papaefstathiou, C. D. Malliakas, I. Papadas, G. S. Armatas, I. Margiolaki, M. G. Kanatzidis, T. Lazarides and M. J. Manos, *Angew. Chem., Int. Ed.*, 2015, **54**, 1651–1656.

7 (*a*) O. M. Yaghi, H. Li, C. Davis, D. Richardson and T. L. Groy, *Acc. Chem. Res.*, 1998, **31**, 474–484; (*b*) M. Eddaoudi, J. Kim, D. Vodak, A. Sudik, J. Wachter, M. O'Keeffe and O. M. Yaghi, *Proc. Natl. Acad. Sci. U. S. A.*, 2002, **99**, 4900–4904.

8 (*a*) X.-L. Zhao and W.-Y. Sun, *CrystEngComm*, 2014, **16**, 3247–3258; (*b*) B. Manna, A. V. Desai and S. K. Ghosh, *Dalton Trans.*, 2016, **45**, 4060–4072.

9 (*a*) S. M. Cohen, *Chem. Rev.*, 2012, **112**, 970–1000; (*b*) O. Karagiaridi, W. Bury, J. E. Mondloch, J. T. Hupp and O. K. Farha, *Angew. Chem., Int. Ed.*, 2014, **53**, 4530–4540; (*c*) E. J. Kyprianidou, T. Lazarides, S. Kaziannis, C. Kosmidis, G. Itskos, M. J. Manos and A. J. Tasiopoulos, *J. Mater. Chem. A*, 2014, **2**, 5258–5266.

10 (*a*) N. Stock and S. Biswas, *Chem. Rev.*, 2012, **112**, 933–969; (*b*) Z.-J. Lin, J. Lü, M. Hong and R. Cao, *Chem. Soc. Rev.*, 2014, **43**, 5867–5895.

11 (*a*) C. N. R. Rao, S. Natarajan and R. Vaidhyanathan, *Angew. Chem., Int. Ed.*, 2004, **43**, 1466–1496; (*b*) E. E. Moushi, A. Kourtellaris, I. Spanopoulos, M. J. Manos, G. S. Papaefstathiou, P. N. Trikalitis and A. J. Tasiopoulos, *Cryst. Growth Des.*, 2015, **15**, 185–193.

12 (*a*) M.-S. Chen, Z.-S. Bai, T. Okamura, Z. Su, S.-S. Chen, W.-Y. Sun and N. Ueyama, *CrystEngComm*, 2010, **12**, 1935–1944; (*b*) X.-J. Deng, W. Gu, L. Wang, L.-F. Zeng and X. Z. Liu, *Z. Anorg. Allg. Chem.*, 2011, **637**, 708–712; (*c*) M.-S. Chen, M. Chen, S. Takamizawa, T. Okamura, J. Fan and W.-Y. Sun, *Chem. Commun.*, 2011, **47**, 3787–3789; (*d*) Y. Xiong, Y.-Z. Fan, R. Yang, S. Chen, M. Pan, J.-J. Jiang and C.-Y. Su, *Chem. Commun.*, 2014, **50**, 14631–14634; (*e*) Z. Chen, K. Adil, L. J. Weselinski, Y. Belmabkhout and M. Eddaoudi, *J. Mater. Chem. A*, 2015, **3**, 6276–6281.

13 (*a*) X. Zhang, Y.-Y. Huang and Y.-G. Yao, *Inorg. Chem. Commun.*, 2013, **28**, 49–51; (*b*) L. Qin, J.-S. Hu, L.-F. Huang, Y.-Z. Li, Z.-J. Guo and H.-G. Zheng, *Cryst. Growth Des.*, 2010, **10**, 4176–4183; (*c*) X. Zhang, J. Cheng, F. Chen, M. Sun and Y. Yao, *Inorg. Chem. Commun.*, 2011, **14**, 358–361; (*d*) M. C. Das and P. K. Bharadwaj, *J. Am. Chem. Soc.*, 2009, **131**, 10942–10949; (*e*) M. C. Das and P. K. Bharadwaj, *Chem. – Eur. J.*, 2010, **16**, 5070–5077; (*f*) A. Karmakar, L. M. D. R. S. Martins, S. Hazra, M. F. C. G. Da Silva and A. J. L. Pombeiro, *Cryst. Growth Des.*, 2016, **16**, 1837–1849; (*g*) M.-H. Xie, X.-L. Yang and C.-D. Wu, *Chem. – Eur. J.*, 2011, **17**, 11424–11427.

14 (*a*) V. Chandrasekhar, C. Mohapatra and R. Metre, *Cryst. Growth Des.*, 2013, **13**, 4607–4614; (*b*) V. Chandrasekhar and C. Mohapatra, *Cryst. Growth Des.*, 2013, **13**, 4655–4658.

15 S. S.-Y. Chui, S. M.-F. Lo, J. P. H. Charmant, A. G. Orpen and I. D. Williams, *Science*, 1999, **283**, 1148–1150.

16 (*a*) V. Guillerm, D. Kim, J. F. Eubank, R. Luebke, X. Liu, K. Adil, M. S. Lah and M. Eddaoudi, *Chem. Soc. Rev.*, 2014, **43**, 6141–6172; (*b*) J. F. Eubank, H. Mouttaki, A. J. Cairns, Y. Belmabkhout, L. Wojtas, R. Luebke, M. Alkordi and M. Eddaoudi, *J. Am. Chem. Soc.*, 2011, **133**, 14204–14207; (*c*) X. Liu, M. Oh and M. S. Lah, *Inorg. Chem.*, 2011, **50**, 5044–5053; (*d*) X. Liu, M. Oh and M. S. Lah, *Cryst. Growth Des.*, 2011, **11**, 5064–5071; (*e*) S. Xiang, J. Huang, L. Li, J. Zhang, L. Jiang, X. Kuang and C.-Y. Su, *Inorg. Chem.*, 2011, **50**, 1743–1748; (*f*) B. Moulton, J. Lu, R. Hajndl, S. Hariharan and M. J. Zaworotko, *Angew. Chem., Int. Ed.*, 2002, **41**, 2821–2824; (*g*) S. A. Bourne, J. Lu, A. Mondal, B. Moulton and M. J. Zaworotko, *Angew. Chem., Int. Ed.*, 2001, **40**, 2111–2113.

17 (*a*) E. J. Kyprianidou, G. S. Papaefstathiou, M. J. Manos and A. J. Tasiopoulos, *CrystEngComm*, 2012, **14**, 8368–8373; (*b*) M. J. Manos, E. J. Kyprianidou, G. S. Papaefstathiou and A. J. Tasiopoulos, *Inorg. Chem.*, 2012, **51**, 6308–6314; (*c*) C. G. Efthymiou, E. J. Kyprianidou, C. J. Milios, M. J. Manos and A. J. Tasiopoulos, *J. Mater. Chem. A*, 2013, **1**, 5061–5069.

18 Oxford Diffraction, *CrysAlis CCD and CrysAlis RED*, Oxford Diffraction Ltd., Abingdon, UK, 2008.

19 M. C. Burla, R. Caliandro, M. Camalli, B. Carrozzini, G. L. Cascarano, L. De Caro, C. Giacovazzo, G. Polidori and R. Spagna, *J. Appl. Crystallogr.*, 2005, **38**, 381–388.

20 G. M. Sheldrick, *Acta Crystallogr., Sect. A: Fundam. Crystallogr.*, 2008, **64**, 112–122.

21 L. J. Farrugia, *J. Appl. Crystallogr.*, 1999, **32**, 837–838.

22 K. Brandenburg, *DIAMOND, Version 2003.2001d*, Crystal Impact GbR: Bonn, Germany, 2006.

23 http://www.ccp14.ac.uk/ccp/web-mirrors/x-seed/.

24 A. L. Spek, *J. Appl. Crystallogr.*, 2003, **36**, 7–13.

25 C. F. Macrae, P. R. Edgington, P. McCabe, E. Pidcock, G. P. Shields, R. Taylor, M. Towler and J. Van De Streek, *J. Appl. Crystallogr.*, 2006, **39**, 453–457.

26 L. Sarkisov and A. Harrison, *Mol. Simul.*, 2011, **37**, 1248–1257.

27 Y. Lin, C. Kong and L. Chen, *RSC Adv.*, 2016, **6**, 32598–32614.

28 Y. Lin, C. Kong and L. Chen, *RSC Adv.*, 2012, **2**, 6417–6419.

29 R. Vaidhyanathan, S. S. Iremonger, K. W. Dawson and G. K. H. Shimizu, *Chem. Commun.*, 2009, 5230–5232.

30 Y. Fu, D. Sun, Y. Chen, R. Huang, Z. Ding, X. Fu and Z. Li, *Angew. Chem., Int. Ed.*, 2012, **51**, 3364–3367.

31 J. Ethiraj, E. Albanese, B. Civalleri, J. G. Vitillo, F. Bonino, S. Chavan, G. C. Shearer, K. P. Lillerud and S. Bordiga, *ChemSusChem*, 2014, **7**, 3382–3388.

32 H. Furukawa, N. Ko, Y. B. Go, N. Aratani, S. B. Choi, E. Choi, A. Ö. Yazaydin, R. Q. Snurr, M. O'Keeffe, J. Kim and O. M. Yaghi, *Science*, 2010, **329**, 424–428.

33 J. Moellmer, A. Moeller, F. Dreisbach, R. Glaeser and R. Staudt, *Microporous Mesoporous Mater.*, 2011, **138**, 140–148.
34 J. M. Simmons, H. Wu, W. Zhou and T. Yildirim, *Energy Environ. Sci.*, 2011, **4**, 2177–2185.
35 V. Guillerm, Ł. J. Weseliński, Y. Belmabkhout, A. J. Cairns, V. D'Elia, Ł. Wojtas, K. Adil and M. Eddaoudi, *Nat. Chem.*, 2014, **6**, 673–680.
36 Y. He, W. Zhou, G. Qian and B. Chen, *Chem. Soc. Rev.*, 2014, **43**, 5657–5678.
37 I. Spanopoulos, C. Tsangarakis, E. Klontzas, E. Tylianakis, G. Froudakis, K. Adil, Y. Belmabkhout, M. Eddaoudi and P. N. Trikalitis, *J. Am. Chem. Soc.*, 2016, **138**, 1568–1574.
38 J.-M. Lin, C.-T. He, Y. Liu, P.-Q. Liao, D.-D. Zhou, J.-P. Zhang and X.-M. Chen, *Angew. Chem., Int. Ed.*, 2016, **55**, 4674–4678.
39 Y. Peng, V. Krungleviciute, I. Eryazici, J. T. Hupp, O. K. Farha and T. Yildirim, *J. Am. Chem. Soc.*, 2013, **135**, 11887–11894.
40 H. Furukawa, M. A. Miller and O. M. Yaghi, *J. Mater. Chem.*, 2007, **17**, 3197–3204.
41 D. P. Broom, C. J. Webb, K. E. Hurst, P. A. Parilla, T. Gennett, C. M. Brown, R. Zacharia, E. Tylianakis, E. Klontzas, G. E. Froudakis, T. A. Steriotis, P. N. Trikalitis, D. L. Anton, B. Hardy, D. Tamburello, C. Corgnale, B. A. Van Hassel, D. Cossement, R. Chahine and M. Hirscher, *Appl. Phys. A*, 2016, **122**, 151.